

## AERODYNAMIC ANALYSIS OF SUPERSONIC FLOW OVER A SIMPLE AIRCRAFT GEOMETRY by USING CST and PANEL METHODS

Levent Uğur<sup>1</sup>, Sena Turan,<sup>2</sup>  
Ramazan Kürşat Gedik<sup>3</sup>, Ali Ata Adam,<sup>4</sup>  
and Nilay Sezer-Uzol<sup>5</sup>  
Middle East Technical University  
Ankara, Turkey

Sercan Ertem<sup>6</sup> and Erdem Ayan<sup>7</sup>  
Turkish Aerospace  
Ankara, Turkey

### ABSTRACT

*In this paper, the aerodynamic properties of a selected aircraft geometry are calculated in supersonic flow condition using PANAIR. PANAIR is an open-source high-order panel method solver for irrotational and inviscid flows and it is more efficient than higher fidelity CFD analyses for the preliminary design process since it is faster and easier to use. A batch of supersonic analyses is completed for different wing/body configurations for the selected aircraft geometry and with various panel grids, and the results are compared with the experimental data. Different wing planforms and nose configurations are also considered separately to observe the effect of geometry to the prediction accuracy of PANAIR. Moreover, a Class-Shape Transformation (CST) code is also developed to create wing and nose geometries together with the surface panel mesh with parametrization. In addition, SU2 and DATCOM software are used to compare the computational results.*

### INTRODUCTION

Panel methods are one of the most convenient ways to solve numerical problems at subsonic and supersonic Mach numbers. These methods are applicable for incompressible flow at subsonic speeds. On the other hand, the approach of PANAIR, an open-source high-order panel method solver developed by Boeing [Carmichael and Erickson, 1981], is capable of obtaining aerodynamics properties at supersonic speeds by solving the Prandtl-Glauert equation for compressible flows. By using high-order singularities, which are the linear source and quadratic doublet distributions, PANAIR can calculate aerodynamic results more accurately than earlier panel methods and faster than finite volume Computational Fluid Dynamics (CFD) solvers [Carmichael and Erickson, 1981]. Due to

<sup>1</sup>Senior Undergraduate Student, Dept. of Aerospace Engineering, METU. Email: levent.ugur@metu.edu.tr

<sup>2</sup>Senior Undergraduate Student, Dept. of Aerospace Engineering, METU. Email: turan.sena@metu.edu.tr

<sup>3</sup>Senior Undergraduate Student, Dept. of Aerospace Engineering, METU. Email: ramazan.gedik@metu.edu.tr

<sup>4</sup>Graduate Research Assistant, Dept. of Aerospace Engineering, METU. Email: adam@metu.edu.tr

<sup>5</sup>Assoc. Prof. Dr., Dept. of Aerospace Engineering, METU. Email: nuzol@metu.edu.tr

<sup>6</sup>Aircraft Engineering, Turkish Aerospace Industries, Inc. Email: sercan.ertem@tai.com.tr

<sup>7</sup>Dr., Aircraft Engineering, Turkish Aerospace Industries, Inc. Email: eayan@tai.com.tr

these advantages of panel methods, their usage becomes popular again [Davis and Marshall, 2020], especially for supersonic cases where inviscid and irrotational flow assumptions are highly valid.

In this study, the geometry to be analyzed, which is 45° sweptback wing with NACA 65A004 airfoil airplane, is generated and meshed using two different methods: CATIA (or OpenVSP)/Pointwise and CST code. The complete geometry is investigated in 3 different configurations: wing only, body only and wing/body. In the first method, the geometry is generated in CATIA and then meshed by using Pointwise. This methodology enables analyzing any specific complex configuration with different geometries including stabilizers and nacelles. However, this process takes a long time, even when a slight change in the geometry or meshing is desired. In the second method, the geometry is generated using Class Shape Transformation (CST) equations. Class Shape Transformation is a commonly used method to prepare aircraft geometries for panel methods. The first reason for this choice is that the number of geometries that can be created by manipulating shape and class functions is numerous. It is even possible to obtain complete aircraft configuration with small, detailed geometry parts as cowl, nacelle and input ramps [Kapania and Sultan, 2014]. This method also provides smooth surfaces, which is an advantage to create leading edge geometries, and provides sharp trailing edges or with desired trailing edge gaps [Kulfan, 2007]. The geometry can also be automatically panelled by using this method decreasing the pre-processing cost of the panel method analysis. To validate PANAIR results further, different nose and wing shapes are also investigated.

PANAIR analyses are completed for the supersonic flow of 2.01 Mach over the geometry, which is generated as explained above, using the convenient boundary conditions for the supersonic flow and solution networks, and the results are compared with the experimental data. Then, a grid refinement study is conducted according to the accuracy of the results with respect to the experimental data. In addition, SU2 CFD [Palacios et al., 2013] and DATCOM [McDonnell Douglas Astronautics Company, 1979] aerodynamic analyses are performed and the results are implemented into the verification study. Finally, the aerodynamic characteristics of 4 different wing configurations with the same reference area are compared by using PANAIR parametric sweep analyses for different flow conditions. The results are compared with SU2 Euler solution and the differences are obtained in the percentage scale to comment on the effect of the wing geometry to the prediction accuracy.

## METHOD

### Theory of PANAIR Code

PANAIR code is based on solving the Prandtl-Glauert equation represented below.

$$(1 - M_\infty^2)\phi_{xx} + \phi_{yy} + \phi_{zz} = 0 \quad (1)$$

This approach assumes steady, compressible, inviscid, irrotational, and isentropic flow. Here, the  $\phi$  term represents perturbation potential defined as;

$$\phi = \Phi - \Phi_\infty \quad (2)$$

where  $\Phi$  and  $\Phi_\infty$  are velocity and freestream potentials, respectively. Then, the velocity,  $V$ , at control points can be evaluated as;

$$\vec{V} = \nabla\Phi = \nabla\Phi_\infty + \nabla\phi = \vec{V}_\infty + \vec{v} \quad (3)$$

where  $V_\infty$  and  $v$  are freestream and perturbation velocities, respectively.

The Prandtl-Glauert equation is manipulated in order to make the equation simpler. This manipulation is based on the following coordinate transformation.

$$\bar{x} = x \quad \bar{y} = Ay \quad \bar{z} = Az \quad (4)$$

where

$$A = \sqrt{|1 - M_\infty^2|} \quad (5)$$

Finally, the simplified equation for supersonic condition in terms of perturbation potential is given as [Carmichael and Erickson, 1981]:

$$-\phi_{xx} + \phi_{yy} + \phi_{zz} = 0 \quad (6)$$

The potentials given in Equation 6 are calculated by integrating source and doublet strengths located on the panels. The potential calculation for supersonic flows is given in Equation 7:

$$\phi(P) = -\frac{1}{4\pi} \iint_S \left( \frac{\sigma}{R} - \mu \vec{n} \cdot \Delta \frac{1}{R} \right) dS \quad (7)$$

In this equation,  $\sigma$  is the source strength,  $\mu$  is the doublet strength and  $P$  represents any point on the flow field. The integral is calculated for the whole surface of the network and the potential is calculated for a point. Since supersonic conditions give a hyperbolic equation, the domain of influence should be implemented correctly to the solution. PANAIR uses the area that lies in the upstream Mach cone of each point for supersonic calculations. This is explained in [Erickson, 1990] in detail.

All boundary conditions of PANAIR can be found in [Saaris, 1992]. The boundary conditions in PANAIR are denoted with a number and assigned to 'kt' variable. Double digit boundary conditions are used for velocity boundary conditions, whereas single digits are used for mass flux boundary conditions. The most used ones are briefly introduced as the following.  $w$  is used for mass flux vector which is defined from compressibility direction.  $v$  is perturbation velocity and  $V_\infty$  is free stream velocity.  $U$  and  $L$  are used to describe the upper and lower surfaces of a panel. Each boundary condition is actually two conditions for upper and lower control points.

$$\vec{W} = \vec{V}_\infty + \vec{w} = \frac{\rho}{\rho_\infty} \vec{V}$$

1. kt=1: Mass flux boundary condition for thick surfaces. Suggested for subsonic flow over wings and bodies.

$$(\vec{w}_U - \vec{w}_L) \cdot \vec{n} = -\vec{V}_\infty \cdot \vec{n}$$

$$\phi_L = 0$$

2. kt=11: Velocity boundary condition for thick surfaces. Suggested for supersonic flow over wing and bodies.

$$(\vec{v}_U - \vec{v}_L) \cdot \vec{n} = -\vec{V}_\infty \cdot \vec{n}$$

$$\phi_L = 0$$

3. kt=5: It is used for fuselage base networks. PANAIR cannot work with a sharp fuselage. Instead of that, a base should be defined and this boundary condition should be given.

$$\vec{w}_U \cdot \vec{n} = 0$$

$$\phi_U = 0$$

4. kt=3&13: These boundary conditions are used for super-inclined panels with a greater angle than the Mach cone. They are defined for mass flux and velocity boundary conditions, respectively.

$$\vec{w}_L \cdot \vec{n} = 0, \quad \phi_L = 0$$

$$\vec{v}_L \cdot \vec{n} = 0, \quad \phi_L = 0$$

5.  $kt=9$ : This boundary condition is used for inlet and exit networks for engines. The mass flux incoming and outgoing can be defined.

$$\vec{w}_U \cdot \vec{n} = -\vec{V}_\infty \cdot \vec{n} - \text{mass flux incoming}$$

$$\phi_L = 0$$

6.  $kt=20$ : This boundary condition is used to define wake networks to connect wing and fuselage networks. This complicated geometry cannot be directly defined in PANAIR. Hence, this boundary condition can be used.

Using Equation 6, 7 and boundary conditions, the linearized governing equation is obtained [Erickson, 1990]. The set of equations can be expressed in the matrix form as

$$[AIC]\{\lambda\} = \{b\} \quad (8)$$

In this equation,  $[AIC]$  is the aerodynamic influence coefficients matrix,  $\lambda$  is the singularity parameters desired to be calculated, and  $b$  vector is the right-hand side matrix that defines boundary conditions. The solution of this matrix solved by LU decomposition gives the singularity parameters, which are used for defining source and doublet strengths [Epton and Mangus, 1990]. Then, by using Equation 7, the velocity potential at any point can be calculated and the flow properties can be obtained by using the potentials.

### Class Shape Transformation (CST)

Class Shape Transformation is a parametric geometry representation method [Kulfan, 2007] which is mainly developed for aerodynamic design considerations. This method is handy for optimization processes since the required parameters to create a geometry are diminished thanks to parametrization. It is even possible to obtain complete aircraft configuration with small, detailed geometries such as cowl, nacelle and input ramps [Kapania and Sultan, 2014]. This method also provides smooth surfaces which is an advantage to create leading edge geometries and provides sharp trailing edges with desired trailing edge gaps [Kulfan, 2007].

In Class Shape Transformation, nondimensionalized coordinate systems are used to simplify the calculations:

$$\psi = x/\text{chord} \quad (9)$$

$$\xi = z/\text{chord} \quad (10)$$

Note that the values of new coordinates are between 0 and 1 along the chordwise direction  $x$  from leading edge to trailing edge for each airfoil section. CST is basically the multiplication of these two functions: Class and Shape. The class function gives the general shape of the geometry, whereas the shape function is a Bernstein polynomial. The order of Bernstein polynomial used in this study is three. As mentioned in [Leal et al., 2019], the mathematical definition of the class function is given in Equation 11 as

$$C(\psi) = \psi^{N_1}(1 - \psi)^{N_2} \quad (11)$$

In general,  $N_1$  and  $N_2$  get 0.5 and 1.0 respectively for airfoil shapes [Giblette, 2019]. The shape function can also be expressed as

$$S(\psi) = a_0 \binom{3}{0} (1 - \psi)^3 + a_1 \binom{3}{1} \psi(1 - \psi)^2 + a_2 \binom{3}{2} \psi^2(1 - \psi) + a_3 \binom{3}{3} \psi^3 \quad (12)$$

Then, the normalized  $z$  coordinates as a function of  $\psi$  can be calculated as

$$\xi(\psi) = \frac{C(\psi)S(\psi)}{4} \quad (13)$$

In this study, the CST method is used to create two parts of the NASA sweptback supersonic test model. These are airfoil geometry and the nose section of the fuselage. First, an inverse process has been completed to get the parameters used in CST calculations. Then, the parameters are used in CST code which gives the model wing geometry with panel mesh directly with or without the fuselage body. The spanwise change of any parameter, such as chord length, dihedral, and twist, is described with a linear change between the selected two end stations as given below:

$$g(\eta) = g_1 + (g_2 - g_1) \frac{\eta}{b} \quad (14)$$

where  $g$  is any parameter that changes in the spanwise direction,  $b$  is span length, and  $\eta$  is normalized spanwise coordinate.  $g_1$  and  $g_2$  is the value of this variable at control end stations and  $\eta$  is an arbitrary point between  $\eta_1$  and  $\eta_2$ .

The body section of the model has a circular cross-section. Hence, the body is created by revolving a reference line around the  $x$ -axis. Since the wing has linear spanwise geometry and the body has circular geometry, the intersection of these two components can be obtained by linear solution of the following two expressions:

$$z^2 + y^2 = r^2 \quad (15)$$

$$z = z_2 + \frac{z_2 - z_1}{y_2 - y_1} (y - y_2) \quad (16)$$

where  $r$  is the local radius of the body cross-section and  $z_1, z_2, y_1, y_2$  are any two known points on the same line of the wing structure.

### Utility Codes

During the analyses, some utility codes are used other than PANAIR main solver code to increase the speed of pre- and post-processes. Some of these codes are obtained from Adam et al [2020] which are **pointwise2panair**, **panINPUT** and **panVISUAL**. The desired geometries can be obtained by openVSP and panelled in Pointwise to obtain the panel mesh. **pointwise2panair** enables transferring gridgen format file which is obtained from Pointwise to a PANAIR mesh format. However, this geometry file cannot be directly used by PANAIR and it should be implemented in the input file. Hence, the other utility code **panINPUT** is used. This code takes parameters that will be used during analysis from the user in a more simple way and unite them with a geometry file. After the pre-processing of the geometry and panel mesh, PANAIR solver is used and the solutions are obtained. When the analysis is completed, **panVISUAL** utility code is used to arrange the outputs in a Tecplot format.

Additional to these codes, new in-house codes are also developed during this study Uğur et al [2020]. **panCST** code is introduced to create geometries in a parametric way with CST method and to panel them automatically. This provides shorter pre-processing time and thanks to the parametric approach, it can be used for optimization processes in future studies. Finally, a framework program, **panBATCH**, is used to perform parametric sweep analyses automatically. It combines **panINPUT**, PANAIR and **panVISUAL** to get Mach, angle of attack or sideslip angle sweep analyses. The code gives aerodynamic coefficients as an output file.

### Description of The Geometry

The geometry considered in the validation studies is the test model used by NASA in the supersonic experiments in a wind tunnel [Gapcynski and Landrum, 1958]. The properties of the wing and body sections are given in Table 1. By using these properties, the simple aircraft geometry obtained from CST is given in Figure 1.

Table 1: Properties of the Test Model

Wing Area [ $in^2$ ]	144.0
Span	24.00 in
Root Chord	10.00 in
Tip Chord	2.00 in
Taper Ratio	0.2
Aspect Ratio	4
Mean Aerodynamic Chord	6.89 in
Quarter Chord Sweep	45 deg
Airfoil Section	NACA 65A004
Incidence	0 deg
Body Length	36.5 in
Diameter (max)	3.33 in
Fineness Ratio	10.96

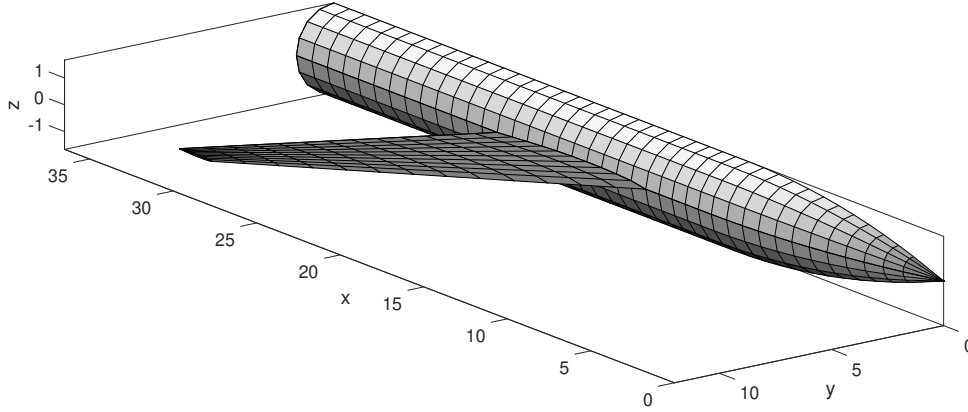


Figure 1: NASA Sweptback Supersonic Test Model obtained from CST

## RESULTS AND DISCUSSION

### Validation Studies

#### Grid Refinement Study:

In grid refinement study, only wing case is considered. Three different meshing are used as coarse, medium and fine meshes for the sweptback wing whose details can be seen in Table 2. These results are for 0 degree angle of attack. It is seen that the grid resolution affects the aerodynamic coefficient results. Since the airfoil is symmetric and the incidence is zero, the expected lift coefficient is zero. Fine meshing has the closest value to that expected value. Another observation is that there is a considerable cost difference between coarse and fine meshes. By using coarse panelling, it is possible to get solutions in less than one second whereas it takes almost thirty minutes for fine mesh. The analyses are completed using one core of Intel(R) Core(TM) i7-7700HQ CPU with 2.8 GHz.

Table 2: Grid Refinement Study

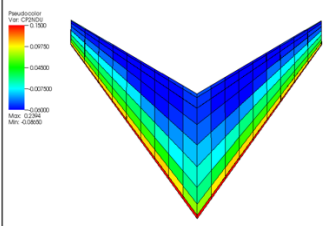
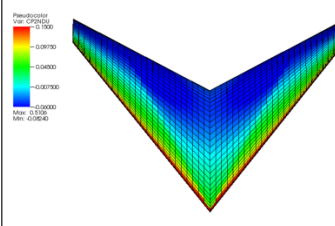
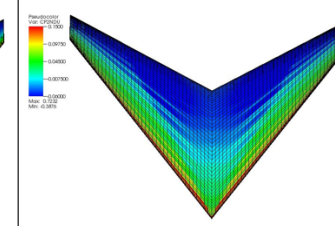
Coarse	Medium	Fine
Chord: 10 grids with cosine spacing Span: 10 grids with uniform spacing	Chord: 30 grids with cosine spacing Span: 25 grids with uniform spacing	Chord: 50 grids with cosine spacing Span: 40 grids with uniform spacing
		
$C_L: -0.00013, C_{Di}: 0.00711$	$C_L: -0.00006, C_{Di}: 0.00801$	$C_L: 0.00001, C_{Di}: 0.00817$
COST = 0.78 sec (0.013 min)	COST = 56.95 sec (0.949 min)	COST = 1758.55 sec (29.31 min)

Figure 2 shows the pressure coefficient distribution results for 0 degree angle of attack solutions. Three different spanwise locations are considered to understand the capability of capturing 3-D effects by PANAIR better. It is obtained that all coarse, medium and fine mesh results are very close. Thus, using coarse mesh does not affect the pressure coefficient distributions so much unlike finite difference/finite volume CFD methods. Also, the fine mesh has some undesired jumps in the solutions. When these results are compared with the experimental results, it is seen that the error at the tip section is more remarkable than the root section. This shows that PANAIR is more successful for predictions without 3-D effects such as flow near the wing tip. In addition, in the experiments, +y and -y represent each wing separately and although there is no sideslip, experimental data of the wings is not precisely the same for both wings.

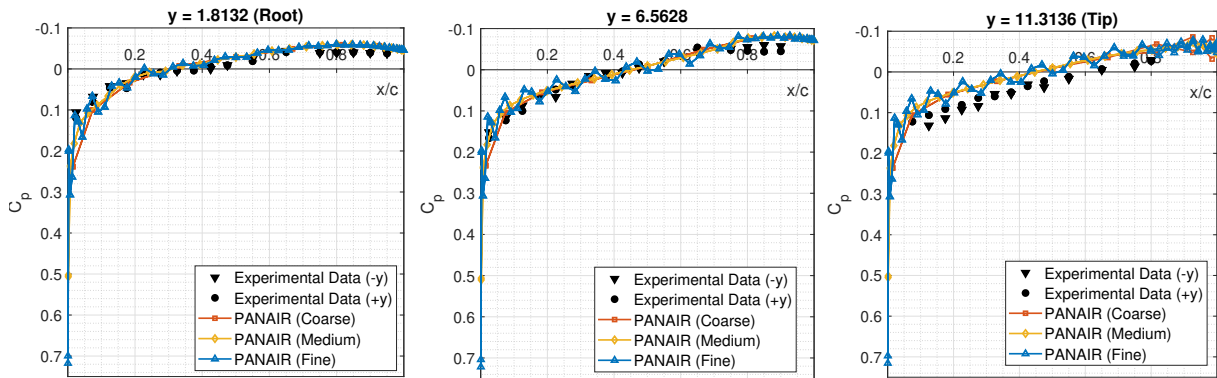


Figure 2: Pressure Coefficient Distributions for Grid Refinement Study at 0° Angle of Attack

Similar observations discussed for 0 degree angle of attack are also valid for 5 degrees as shown in Figure 3. The error increases as the section gets closer to the tip due to 3-D effects.

From this study, it is seen that fine mesh creates undesired jumps due to numerical errors. Coarse and medium meshes give similar and accurate results. However, the medium panel mesh has more points, enabling more smooth and accurate results at the trailing and leading edges. The computational cost of this mesh is also moderate. Hence, the medium mesh is used during the analyses.

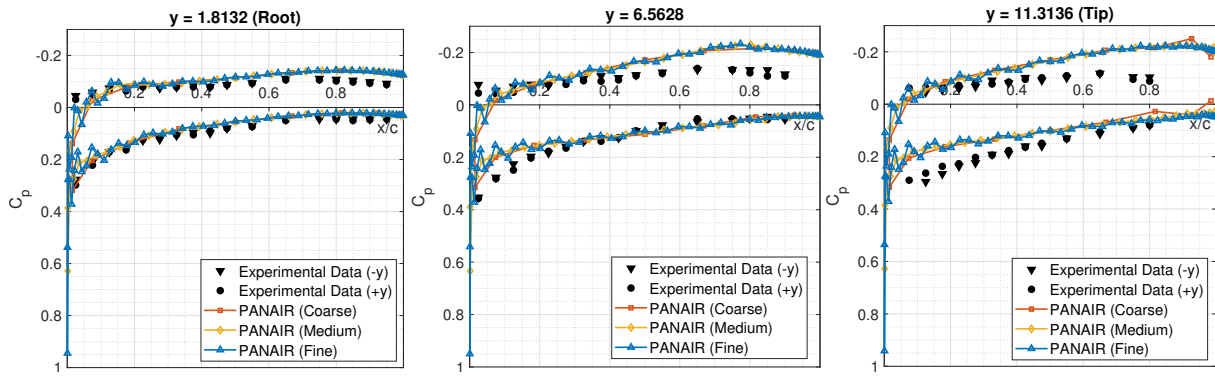


Figure 3: Pressure Coefficient Distributions for Grid Refinement Study at  $5^\circ$  Angle of Attack

### Only Wing Analysis:

Only wing analyses are completed for the 3-D model of the wing section without the fuselage. To validate the results, SU2 [Palacios et al., 2013] Euler solution is also considered to better analyze the accuracy of PANAIR over other inviscid solvers. These computational results are compared with the experimental data for 0 and 5 degrees angle of attack solutions. The pressure distributions are obtained for tip and root sections of the wing to observe the 3-D effects on the results.

Figure 4 shows the pressure coefficient distribution over the chord length for root and tip sections of the wing at zero angle of attack case. Since a symmetric airfoil is used without the appearance of incidence angle, the pressure distributions of lower and upper surfaces are identical for zero angle of attack solution. The root section gives very similar results for the Euler and PANAIR solutions with the experimental data. When the tip section pressure distribution is considered, it is seen that there is a slight difference between computational and experimental results. Some measurement errors might cause this difference. Nevertheless, an error at the tip section is also expected since the flow in this region is under the 3-D effects which gives an unsteady behavior to the solution [Rossow, 1976] which cannot be modeled by steady solvers. Yet, the close results of PANAIR and Euler solutions show that PANAIR has the ability of predicting symmetrical wing case solutions for supersonic flow condition at low angle of attack.

Then, a moderate angle of attack case with 5 degrees is considered on the same geometry. Figure 5 shows the results of this case for the root and tip sections. For root section, the pressure distribution results for each case are very similar, although there are minimal differences between PANAIR and other data at leading and trailing edge locations. However, it can be seen that this minor error gets more prominent when the spanwise section gets closer to the wing tip. This result does not affect the aerodynamic coefficients dramatically since the trends are similar but there is a significant difference between sectional pressure distributions.



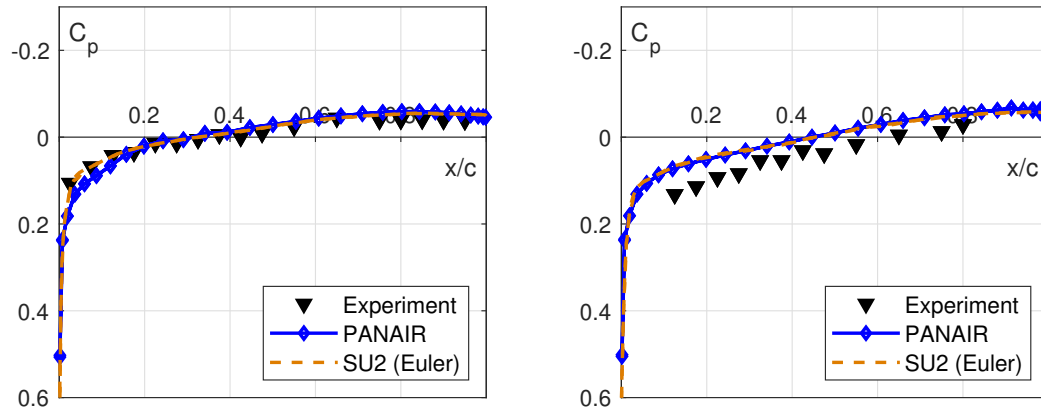


Figure 4: Pressure Coefficient Distributions for Only Wing Analysis at  $0^\circ$  Angle of Attack (Left: Root Section, Right: Tip Section)

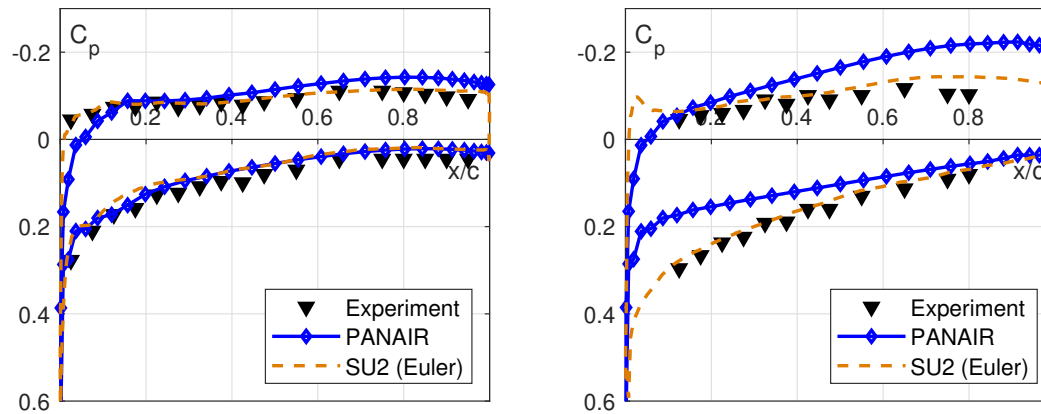


Figure 5: Pressure Coefficient Distributions for Only Wing Analysis at  $5^\circ$  Angle of Attack (Left: Root Section, Right: Tip Section)

To increase the accuracy, the boundary conditions used in the simulations are also changed in this study. The velocity boundary condition ( $kt=11$ ) used during the analyses, which is also recommended for supersonic solutions by the user manual [Saaris, 1992], is changed with a combination of super-inclined ( $kt=3$ ) and mass flux ( $kt=1$ ) boundary conditions. Super-inclined boundary condition is only applied to the first three panels on each surface (upper and lower) and the remaining panels use mass flux boundary condition. The effect of this new combination can be seen in Figure 6. This combination gives much more accurate results than recommended supersonic boundary condition. Super-inclined boundary condition gives zero pressure coefficient without disturbing the flow and it is not able to predict stagnation jump. However, after that region, the solution that uses the mass flux boundary condition gives very accurate results compared with the experimental data.

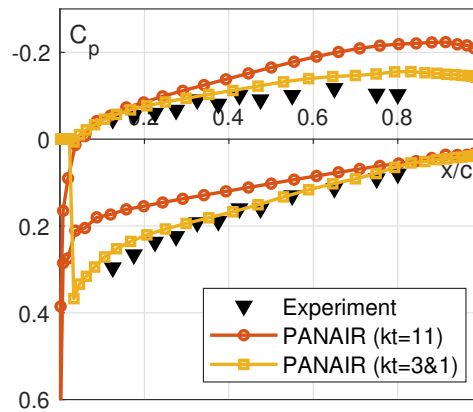


Figure 6: Different Boundary Condition Results for Only Wing Analysis at  $5^\circ$  Angle of Attack

#### Only Body Analysis:

After completing only wing analyses, only body analyses are performed. For the symmetrical body geometry, SU2 [Palacios et al., 2013] Euler solution is also considered, as in only wing analyses, to compare the PANAIR results with SU2 CFD results. Pressure coefficient values of the body are obtained by using both PANAIR and SU2 [Palacios et al., 2013], then they are compared with the experimental data at the nose and tail sections of the body for 0 degree angle of attack.

As can be seen from Figure 7, the pressure coefficient distribution found by PANAIR is close to both SU2 [Palacios et al., 2013] results and experimental data. Since the body geometry is symmetrical and analyses are conducted with 0 degree angle of attack, the pressure coefficient results are expected to be symmetrical and constant over the body. Although PANAIR results are matching with the expectation, both SU2 [Palacios et al., 2013] results and experimental data have changes in the pressure distribution over the body. This can be caused by 3-dimensional flow over the body and flow separations that PANAIR cannot catch. Also, it should be noted that each PANAIR analysis is completed in less than 6 seconds, which is much faster in comparison to CFD analyses.

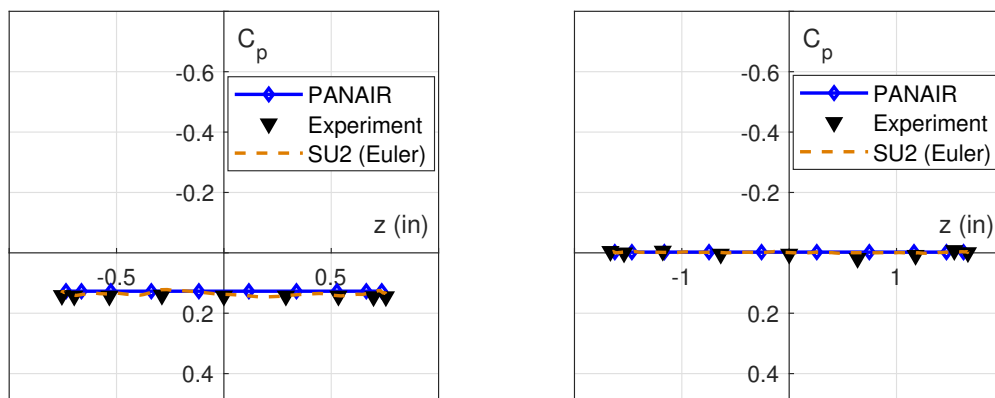


Figure 7: Pressure Coefficient Distributions for Only Body Analysis at  $0^\circ$  Angle of Attack (Left: Nose Section, Right: Tail Section)

In addition, DATCOM [McDonnell Douglas Astronautics Company, 1979] aerodynamic software, which can make fast aerodynamic calculations by interpolating from its own database for a given aircraft geometry, is also used to compare lift coefficient results. As can be seen from Figure 8, while lift coefficient results are very close at small angles of attack, the difference is getting more significant as the angle of attack increases. Since PANAIR is based on linear theory, it is expected

that it gives less accurate results for high angles of attack.

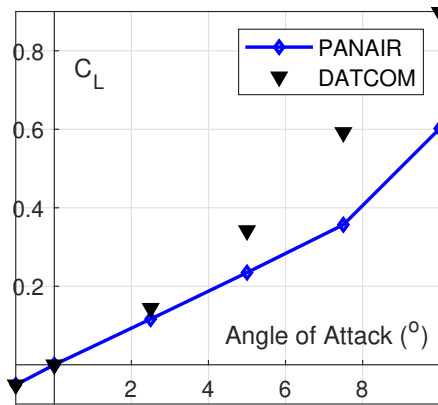


Figure 8: Lift Coefficient Results for Only Body Analysis

#### Wing/Body Analysis:

Finally, for the same wing and body geometries used in the experiment and separately investigated above, complete wing/body geometry is considered in the analyses. Pressure coefficient results obtained by PANAIR analyses are compared with the experimental data at the mid and tail sections of the body. Note that the mid section is just ahead of the wing. PANAIR analyses are done for 0 and 5 degrees of angle of attack cases.

Figure 9 and Figure 10 show the pressure coefficient distributions over the body for 0 degree and 5 degrees of angle of attack cases, respectively. Since the whole wing/body geometry is also symmetric, it is expected to get symmetric and constant pressure coefficient distribution around the body when the angle of attack is 0 degree (Figure 9). Although PANAIR results meet this expectation, the experimental data has small variations. Hence, the same situation explained under the only body analyses section above applies here as well. As can be seen from Figure 10, when the angle of attack becomes 5 degree, while the pressure coefficient results of PANAIR are similar with the experimental data at the mid section, PANAIR gives very different results at the tail section, especially at the region where the wing coincides with the body.

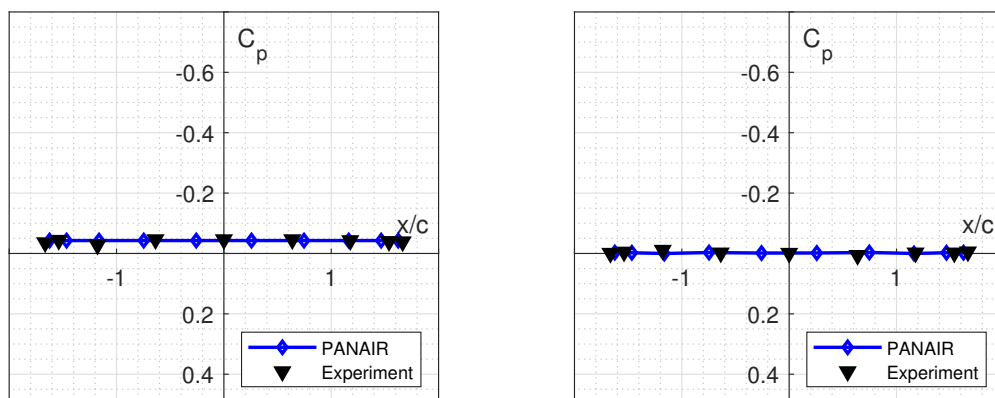


Figure 9: Pressure Coefficient Distributions for Wing/Body Analysis at 0° Angle of Attack (Left: Mid Section, Right: Tail Section)

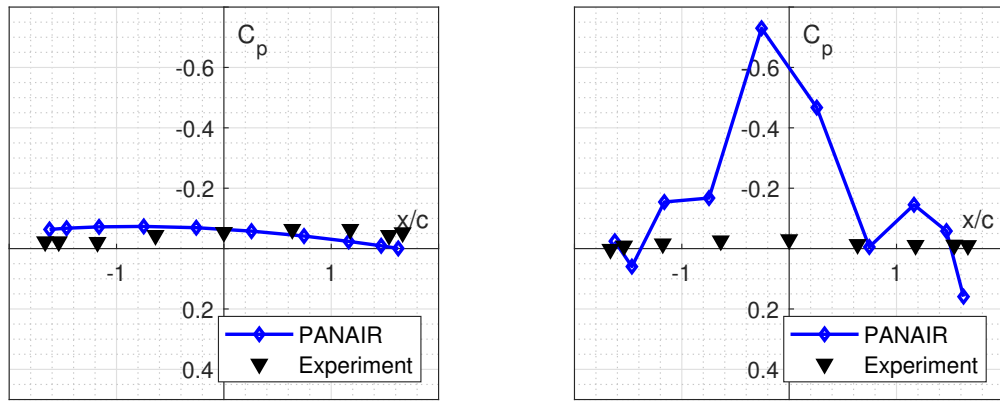


Figure 10: Pressure Coefficient Distributions for Wing/Body Analysis at  $5^\circ$  Angle of Attack (Left: Mid Section, Right: Tail Section)

Finally, the lift coefficient results of PANAIR are also compared with the DATCOM [McDonnell Douglas Astronautics Company, 1979] results to check whether the difference in the pressure coefficient distribution mentioned above affects other aerodynamic coefficients or not. As can be seen from Figure 11, the lift coefficient results are very close, even though the difference is getting larger as the angle of attack increases, which is expected since PANAIR is based on linear theory. Hence, it can be concluded that the difference in the pressure coefficient distribution does not affect lift coefficient results considerably.

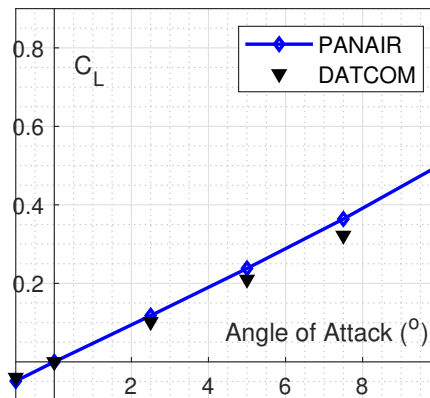


Figure 11: Lift Coefficient Results for Wing/Body Analysis

#### Different Nose Configurations:

The performance of PANAIR calculating lift coefficient is also investigated for different nose configurations at supersonic flow condition. The nose geometries shown in Figure 12 are used and the computations are done with varying angles of attack and Mach number of 2.75 and the results are compared with the available experimental data [Dennis and Cunningham, 1952].

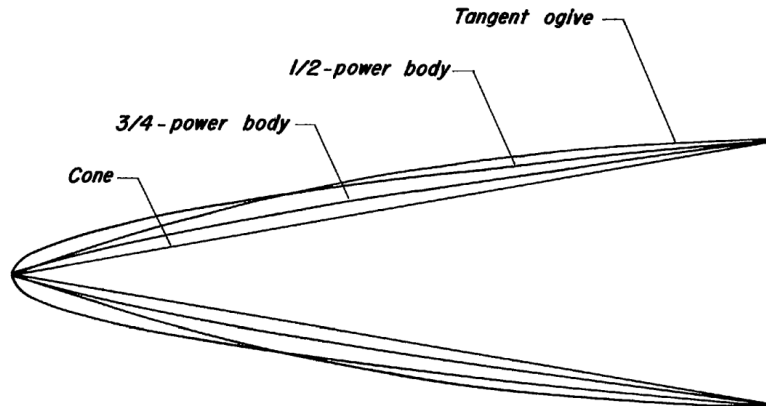


Figure 12: Visualization of Different Nose Configurations Used in Analyses

The nose geometries are drawn by the equation given below:

$$r = r_b \left( \frac{x}{l} \right)^n \quad (17)$$

where,  $l$  and  $r_b$  are the length and the base radius of the geometry, respectively. Longitudinal distance is represented by  $x$ , and the corresponding radius is  $r$ . Cone shape is drawn by  $n = 1$  and power body shape is by  $n = 1/2$ . Tangent ogive shape is drawn by following equation:

$$r = \sqrt{\rho^2 - (l - x)^2} + r_b - \rho \quad (18)$$

$$rho = \frac{r_b^2 + l^2}{2r_b} \quad (19)$$

All analyzed geometries have a base diameter of 1 inch and their lengths vary with different fineness ratios. The fineness ratio is defined as the ratio of length to diameter:

$$f = \frac{l}{r_b} \quad (20)$$

For different nose geometries, the lift coefficients for different angle of attack values are shown in Figures 13, 14 and 15. From Figures 14 and 15, it can be said that by increasing of fineness ratio, the results of PANAIR and the experiment data get closer to each other. This is because linear supersonic theory gives more accurate results for a slender body. In other words, a greater fineness ratio means more slenderness. On the other hand, this effect is not obvious for cone shape 13. The reason might be that the cone shape is a straightforward geometry, so this effect may not be observed. The accuracy of the PANAIR solution is quite obvious at low angle of attack, and as the angle of attack increases the PANAIR solution and experiment start to differ. Also, there is a difference in lift curve slope as well between the PANAIR results and experimental data. The nose of the primary geometry has the same shape as the tangent ogive. Therefore, this study helps to validate calculating lift coefficient for the nose part of the primary model as well.

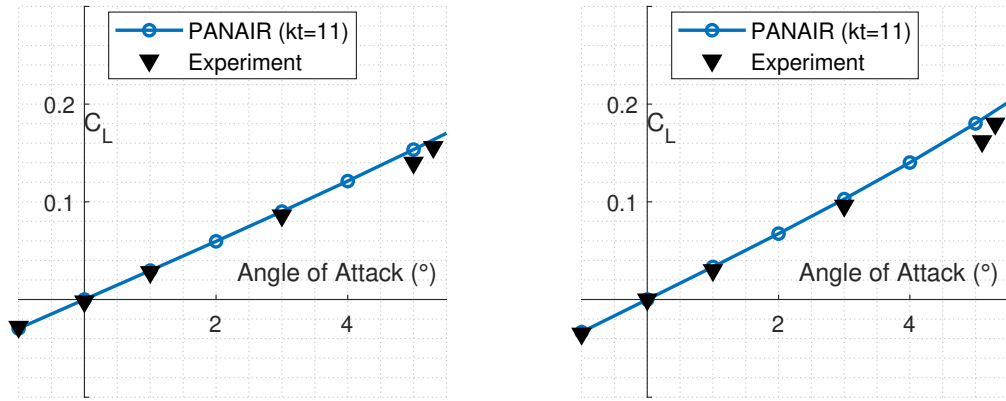


Figure 13: Lift Coefficient Results for Cone Bodies with Different Fineness Ratios of 3 (left) and 7 (right)

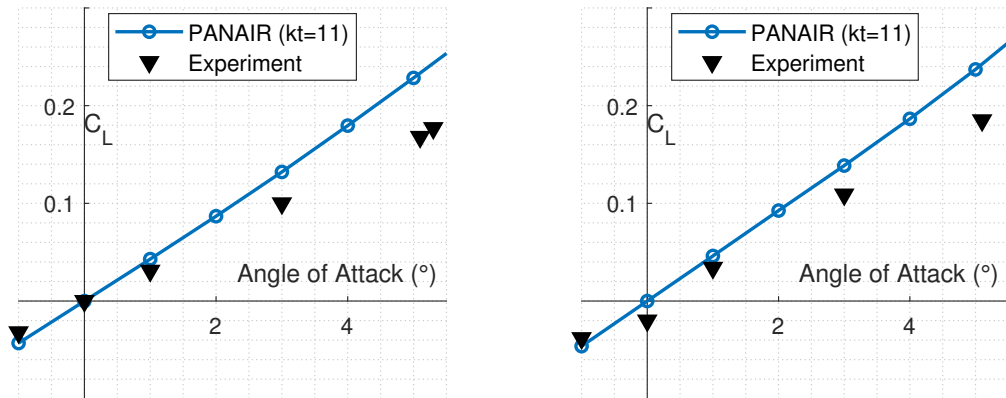


Figure 14: Lift Coefficient Results for Power Bodies with Different Fineness Ratios of 3 (left) and 5 (right)

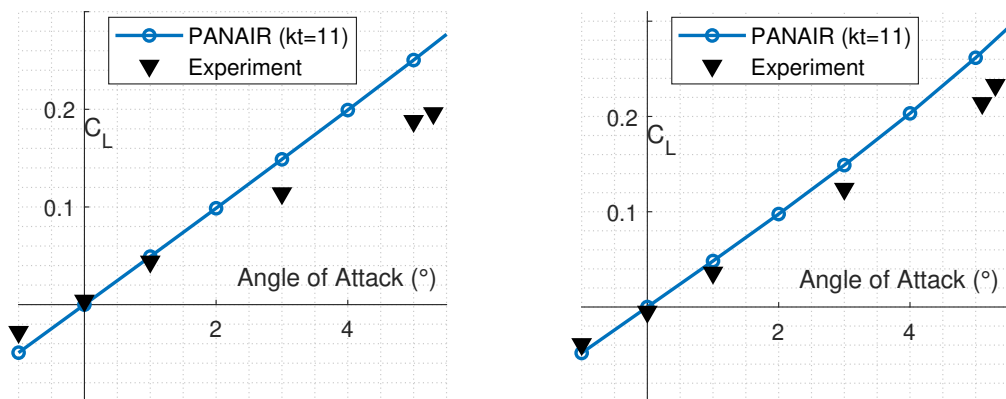


Figure 15: Lift Coefficient Results for Tangent Ogive Bodies with Different Fineness Ratios of 3 (left) and 7 (right)

### Analyses of Different Wing Configurations

After the validation studies, different wing planforms are analyzed using PANAIR, and their aerodynamic performance in the supersonic flow is examined. Four different wing platforms are chosen: sweptback, delta, forward swept, and trapezoidal wings, which are generally used for supersonic aircraft.

#### Properties of the Wings:

The properties of the selected wings are given in Table 3. The wing planform area is taken as constant as  $17.5 \text{ m}^2$  for each wing. The sweptback and forward swept wings are identical except for their sweep angle direction and the sweep angle location is considered as the leading edge for all configurations. Every wing uses NACA 65A004 airfoil, and the analyses are done for 2.0 Mach similar to the validation studies. The visualizations of wing configurations with different planforms are given in Figure 16.

Table 3: Wing Configuration Properties for Analyses

Wing Type	Area[m <sup>2</sup> ]	Span[m]	Sweep[deg]	AR	Taper Ratio	Tip Chord[m]	Root Chord[m]	Ave. Chord[m]
Sweptback	17.5	8.26	35	1.95	0.5	1.41	2.82	2.12
Delta	17.5	5.19	58.5	1.0	0.1	0.54	5.38	2.96
Forward Swept	17.5	8.26	-35	1.95	0.5	1.41	2.82	2.12
Trapezoidal	17.5	5.92	40	1.25	0.25	1.06	4.23	2.65

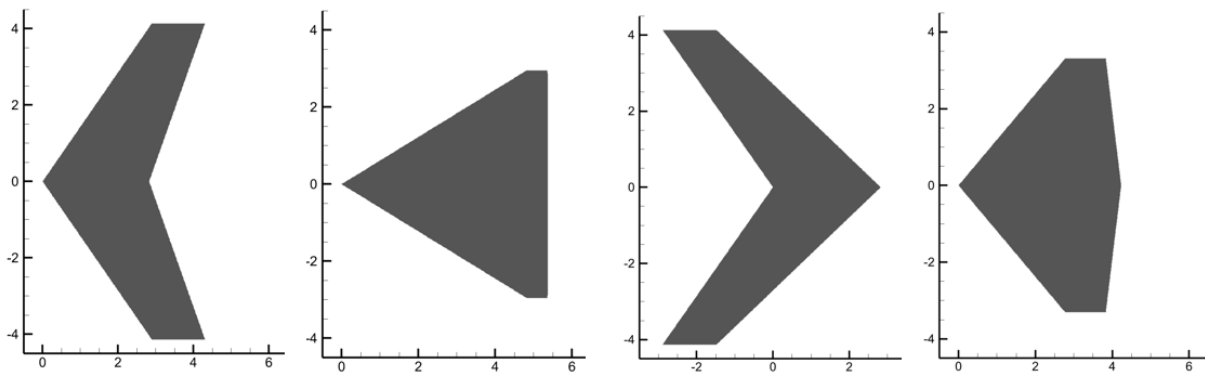


Figure 16: Wing Planform Visualizations for Analyses (Left to Right: Sweptback, Delta, Forward Swept, Trapezoidal)

#### Results of PANAIR Analysis:

The PANAIR analyses are performed by using panBATCH parametric sweep analyses framework. The aerodynamic coefficients are obtained for varying angle of attack values for all configurations. Figure 17 gives the results for lift coefficient for different angle of attack values. The lift curve obtained is linear for given low angle of attack range for all wings because of the linear theory used. It is seen that the sweptback and forward swept wing give higher lift value than the delta and trapezoidal wings, where swept forward wing also gives slightly higher lift coefficient. The lift performance of delta and trapezoidal wings are very similar. The drag coefficient results are also given in Figure 17. It can be seen that the sweptback and forward swept wings that have greater lift coefficient values have greater drag as well. The drag performance of trapezoidal and delta wings are very similar.

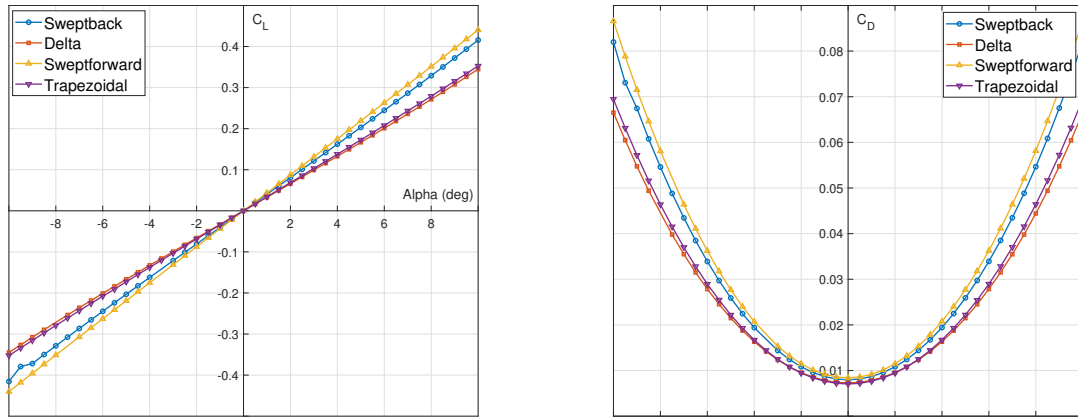


Figure 17: Lift Coefficient (left) and Drag Coefficient (right) versus Angle of Attack for Different Wing Configurations

To better examine the performance of wings, lift to drag ratio is also considered as an important aerodynamic performance coefficient. Figure 18 shows lift coefficient versus drag coefficient (lift-drag polar) which can give an idea about lift to drag performance. It is seen that all results are close to each other. Sweptback and swept forward wings give better performance, where delta and trapezoidal wings give entirely identical results. Swept forward wing has slightly better lift to drag performance.

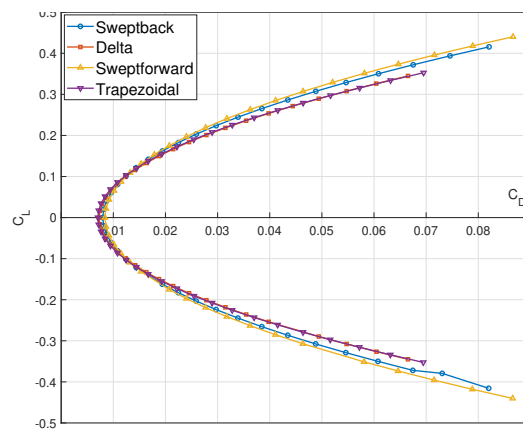


Figure 18: Lift Coefficient versus Drag Coefficient for Different Wing Configurations

Figure 19 shows the pitching moment coefficients of the wing configurations for different angle of attack values. The moment calculation is done with respect to the quarter chord location of the mean aerodynamic chord of the wing. The slope of the pitching moment curve for the given angle of attack range gives the longitudinal pitch up stability of the wing. It is seen that the forward swept wing gives a much more stable behavior than other wings, which mostly requires canard in configurations to relax the longitudinal stability [Clarke et al., 1995]. On the other hand, delta wing gives the least stable pitching moment performance. Moreover, trapezoidal and sweptback wings give similar characteristics for stability.



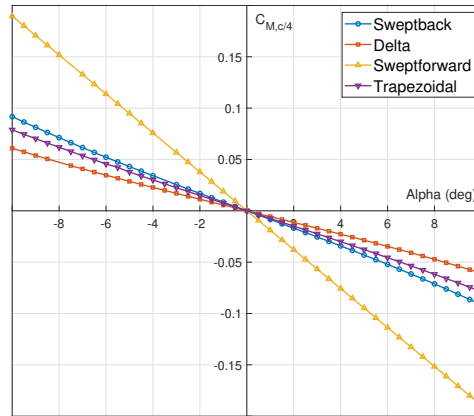


Figure 19: Pitching Moment Coefficient versus Angle of Attack for Different Wing Configurations

#### Comparison of SU2 and PANAIR Results:

Parametric sweep analyses for flow conditions with different angles of attack are also performed by using SU2 Euler CFD solver to obtain a better idea about the solution accuracy of PANAIR for very different wing configurations (or planforms) at Mach number of 2.0. Same meshing scheme is employed for all wing configurations by using nearly 100 nodes on the upper and lower surfaces and 170 nodes along the span with grid clustering at the leading and trailing edges. The half wing with largest span of 8.26 m is placed in the half sphere computational domain with 400 m diameter in size with about 443,000 total number of unstructured tetrahedral cells. The 3-D grid is generated by using Pointwise. The lift and drag coefficients for the wings are obtained for 5 degrees angle of attack by using both PANAIR and SU2. Additionally, lift coefficient slopes by using two angle of attack values (from 0 to 5 degrees) are calculated to observe the accuracy of aerodynamic derivative predictions of PANAIR. The results and the errors of PANAIR prediction with respect to the Euler solution are given in Table 4.

Table 4: Comparison of Aerodynamic Coefficients Obtained from PANAIR and SU2 for 5° Angle of Attack for Different Wing Configurations

	Sweptback			Delta			Forward Swept			Trapezoidal		
	PAN. <sup>a</sup>	SU2 <sup>b</sup>	Diff. <sup>c</sup>	PAN.	SU2	Diff.	PAN.	SU2	Diff.	PAN.	SU2	Diff.
$C_L$	0.203	0.196	3.83%	0.167	0.176	5.27%	0.219	0.202	8.04%	0.173	0.185	6.51%
$C_D$	0.026	0.028	6.32%	0.021	0.020	5.45%	0.028	0.029	2.91%	0.022	0.026	14.08%
$C_{L_\alpha}$	0.041	0.039	3.80%	0.033	0.035	4.93%	0.044	0.041	8.09%	0.035	0.037	6.73%

a: PANAIR, b: SU2 Euler Solution, c: Difference between PANAIR and SU2 results in percentage

Table 4 shows that the prediction differences between PANAIR and SU2 results are between nearly 3-14% when they are compared in percentage. The biggest difference of 14% is for the drag coefficient result of the trapezoidal wing at 5 degrees angle of attack. Other predictions for both lift and drag give differences less than 10%. However, having higher difference percentages for lift, does not mean higher differences in drag predictions. The prediction of lift coefficient of PANAIR gives over-predicted results for sweptback and forward swept wing configurations whereas it predicts less lift value for delta and trapezoidal wings compared to SU2 results. Therefore, during a design optimization study, a simple lift correction for numerical predictions may not easily be applied to represent very different wing planform geometries as simulated here. On the other hand, panel method results show smaller drag coefficients than Euler solutions except for delta wing analysis. Lift curve slope is also considered for comparisons over different wing planforms. It is seen that lift coefficient and lift curve slope prediction differences are close to each other and they are varying in the range of nearly 3-8%. Further analyses of flow characteristics are needed for each wing planform

to understand the cause of differences in predictions by using the different aerodynamic approaches for the given flow conditions in terms of numerical approach and possible numerical errors.

## CONCLUSIONS

In this paper, the aerodynamic analyses are performed by using PANAIR panel code with new pre- and post-processing utility codes, and also by using SU2 CFD solver and DATCOM aerodynamic software for different selected aircraft wing/body configurations in supersonic flow, and the results are compared with the available experiments and with each other.

First, for validation studies, the aerodynamic analyses for the selected model of a simple aircraft geometry are performed by using both CST method and PANAIR panel method code. The aerodynamic simulations for different test cases: a sweptback wing, a cylindrical body and a wing/body geometries, are performed using PANAIR for compressible flow solutions at supersonic condition of  $M = 2.01$ . The geometry and mesh generations by using available solid modeling and mesh generation software and an easy to use and fast in-house CST code are discussed in detail. The grid refinement study for the sweptback wing only case and the validation studies for 0 and 5 degrees angles of attack for all test cases are presented, the results are compared with the available experimental data and discussed. CFD and DATCOM analyses are also performed and comparisons with the PANAIR results are done. Wing analyses show that the error of PANAIR solution increases near the wing tip and as the angle of attack increases because of the limits of linear theory used. To decrease that error, a boundary condition combination is suggested and used for PANAIR analysis, which gives more accurate results on pressure coefficient distribution. It is seen that adding body to the solution increases the error of pressure coefficient distribution. However, this situation does not affect the aerodynamic coefficient results dramatically which is also validated with DATCOM results. Different nose configuration results show the effect of fineness of the geometry to the accuracy of the solution. As the body gets slender, the accuracy of the panel method based on Prandtl-Glauert equation increases. The nose analyses also show that PANAIR can predict aerodynamic coefficients of geometries with great base areas which can be a challenging case for finite volume or finite element solvers.

Then, the aerodynamic characteristics of different selected wing planform configurations are compared by using PANAIR to test the capability of PANAIR for such different configurations. The results are also compared with Euler solutions and the differences between the predictions with these different aerodynamic approaches are calculated. The aerodynamic coefficient results obtained show differences less than 10% between SU2 and PANAIR predictions. Hence, it can be said that parametric wing analysis by using PANAIR during design study of different wing configurations is possible for a certain prediction accuracy. In a parametric design study, PANAIR analyses can be completed in less than 2 minutes which is noticeably faster than Euler solution. The rapidness and also the accuracy of PANAIR analyses for complex 3-D aircraft geometries in supersonic flow condition show that it is still a good alternative numerical approach for aerodynamic optimization and preliminary design processes.

## ACKNOWLEDGEMENT

Part of this study was supported by Turkish Aerospace Lift UP Projects 2020-2021 (Project No: 20201111J13102). Part of this study was also supported by METU AdımODTÜ Projects 2020-2021 (2021 AdımODTÜ Lisans Araştırma Projesi (B6)).

## References

Adam, A.A., Sezer-Uzol, N., Ertem, S., Ayan, E. (2020) *Aerodynamic Analysis of Different Wing/Body Configurations by using Panel Method / Farklı Kanat/Gövde Kon-*

- figürasyonlarının Panel Metodu ile Aerodinamik İncelenmesi (Turkish)*, Mühendis ve Makina Guncel, Nov 2020.
- Carmichael, R. and Erickson, L. (1981) *PAN AIR - A higher order panel method for predicting subsonic or supersonic linear potential flows about arbitrary configurations*, AIAA 14th Fluid and Plasma Dynamics Conference , June 1981.
- Clarke, R., Burken, J.J., Bosworth, J.T. and Bauer, J.E. (1995) *X-29 Flight Control System: Lessons Learned*, International Journal of Control 59(1), June 1995.
- Davis J.D., Marshall, D.D. (2020) *A Higher-Order Method Implemented in an Unstructured Panel Code to Model Linearized Supersonic Flows*, AIAA Science and Technology Forum and Exposition, Orlando, Florida, 6-10 January 2020.
- Dennis, D.H., Cunningham, B.E. (1952) *Forces and Moments on Pointed and Blunt-nosed Bodies of Revolution at Mach Numbers from 2.75 to 5.00* , NACA Research Memorandum, 1952.
- Epton, M. A., Magnus, A. E. (1990) *PAN AIR - A computer program for predicting subsonic or supersonic linear potential flows about arbitrary configurations using a higher order panel method volume I - Theory document (version 3.0)*, NASA Report, 1990.
- Erickson, L. L. (1990) *Panel methods: An introduction*, NASA Technical Publication, Dec 1990.
- Gapcynski, J. P., and Landrum, E. J. (1958) *Tabulated Data from a Pressure-Distribution Investigation at Mach Number 2.01 of a 45 Degrees Sweptback-Wing Airplane Model at Combined Angles of Attack and Sideslip Angle*, NASA Langley Research Center Technical Paper, 1958.
- Giblette, T.N. (2019) *Rapid Prediction of Low-Boom and Aerodynamic Performance of Supersonic Transport Aircraft Using Panel Methods*, Master of Science Thesis, Mechanical Engineering, Utah State University, 2019.
- Kapania, R. and Sultan, C. (2014) *Parametric Geometry Model for Design Studies of Tailless Supersonic Aircraft*, Journal of Aircraft, Sep 2014.
- Kulfan, B. M. (2007) *“CST” Universal Parametric Geometry Representation Method With Applications to Supersonic Aircraft*, Fourth International Conference on Flow Dynamics, Sep 2007.
- Leal, P. B., Giblette, T., Hunsaker, D. F., and Hartl, D. J. (2019) *Extended 3-D Class/Shape Transformation Equations for Multicomponent Aircraft Assemblies*, AIAA Scitech 2019 Forum, 2019.
- McDonnell Douglas Astronautics Company (1979) *The USAF Stability and Control DATCOM, Volume I, Users Manual*, McDonnell Douglas Astronautics Company, 1979.
- Palacios, F., Colonno, M., Aranake, A., Campos, A., Copeland, S., Economon, T., Lonkar, A., Lukaczyk, T., Taylor, T., Alonso, J. (2013) *Stanford University Unstructured (SU2): An open-source integrated computational environment for multi-physics simulation and design* , 51st AIAA Aerospace Sciences Meeting, 2013.
- Roscow, V.J.(1976) *Inviscid modeling of aircraft trailing vortices* , Ames Research Center, 1976.
- Saaris, G. R. (1992) *A502 User’s Manual-PAN AIR Technology Program for Solving Problems of Potential Flow about Arbitrary Configurations* , Boeing Technical Document, 1992.
- Uğur, L., Turan, S., Gedik, R.K., Sezer-Uzol, N., Ertem, S., Ayan, E. (2021) *Supersonic Aerodynamic Analysis and Validations by using PANAIR Panel Method Code / Sesüstü Aerodinamik Analizlerin PANAIR Panel Metodu Kodu ile Yapılması ve Doğrulanması (Turkish)*, Lift UP Project Presentations, 1 July 2021.